Biomineralization: A new tool for developing eco-sustainable Ti-doped hydroxyapatite-based hybrid UV filters

Biomineralization: a new tool for developing eco-sustainable Ti-doped hydroxyapatite-based hybrid UV filters

Elisabetta Campodoni[a], Margherita Montanari[a], Chiara Artusi[a], Linda Bergamini[a], Giada Bassi[a], Elena Destro[b], Ivana Fenoglio[b], Silvia Panseri[a], Anna Tampieri[a], Alessandra Sanson[a], Monica Sandri[a*]*

Pre-print version

Biomineralization: a new tool for developing eco-sustainable Ti-doped hydroxyapatite-based hybrid UV filters

Elisabetta Campodoni[a], Margherita Montanari[a], Chiara Artusi[a], Linda Bergamini[a], Giada Bassi[a], Elena Destro[b], Ivana Fenoglio[b], Silvia Panseri[a], Anna Tampieri[a], Alessandra Sanson[a], Monica Sandri[a*]*

[a.]Institute of Science and Technology for Ceramics-National Research Council (ISTEC-CNR), Faenza, Italy

[b] affiliation

Nowadays, the concern about the damage that solar radiation, especially the ultraviolet component (UVA and UVB), can cause to the skin is constantly growing. In this regard, the use of sunscreens as protective barriers, absorbing or reflecting harmful UVA and UVB rays, is becoming an increasingly important issue. In this work, innovative biomimetic hybrid phases with sunscreen properties were successfully developed and investigated, exploiting the excellent potential and safety of hydroxyapatite nanoparticles. This, with the aim of having new eco-sustainable mineral filters suitable to replace TiO_2 and ZnO commonly used in sunscreen products and that have proven to be not completely safe for humans and marine ecosystems. Through a nature inspired biomineralization process, the selected active phase, titanium-doped hydroxyapatite (TiHA), was nucleated on two different natural organic matrices, gelatin (Gel) and alginate (Alg), to obtain

biomimetic hybrid phases (GelTiHA and AlgTiHA), proving to be active as physical UV filters, not photoreactive, eco-sustainable, and with morphological characteristics that avoid permeation into deeper skin layers. The materials features were investigated in terms of particles shape and nanostructure (SEM), chemical and physical properties (XRD, FTIR, TGA, ICP-OES, DLS) as well as the interaction with UV-VIS radiations (adsorption and reflection spectra), and photodegradation potential. Above all, was demonstrated that both hybrid materials (GelTiHA and AlgTiHA) have excellent reflectance and absorption properties also by virtue of the well-known optical properties of the titanium ion (Ti(IV)). In addition, since titanium is not present in form of titanium dioxide (TiO_2), but as Ti(IV) ion whithin the crystal lattice of hydroxyapatite particles, samples did not highlight photocatalytic effects, an import issue in avoiding the degradation of sunscreens ingredients that would lead to the generation of free radicals or reactive species under sun exposure, harmful for the skin and corals. To conclude, we have developed new mineral filters based on TiHA, which have proved to be effective, biocompatible and biodegradable, and therefore eco-sustainable, thus being safe for human health and the environment.

1. Introduction

The sunlight is essential for our well-being, it is responsible for regulating our internal clock, stimulate metabolism, the hormonal and the immune systems, furthermore, it is essential for the production of vitamin D and therefore for healthy bones. However, excessive exposure to the sun can also be dangerous, especially its ultraviolet (UV) component, that can cause serious damages to both environment and people.

In particular, being the most "energetic" component of the solar spectrum, UV radiation results to be particularly dangerous for human health, especially for skin tissue.(Smaoui et al., 2017) Damaging effects of UV radiation on skin are especially due to generation of reactive oxygen

species (ROS), which cause oxidation of nucleic acids, proteins, and lipids, resulting in photo-aging, photo-carcinogenesis, sunburn, dermatitis, immune-suppression and, ultimately, skin cancer.(Rünger, 1999) UV region falls in the 100-400 nm wavelength range and it is divided into three classes, UVA (320-400 nm), UVB (290-320 nm), and UVC (100-290 nm).(Qian et al., 2017) The most dangerous class are UVC, but thanks to the stratosphere gases, they are prevented from reaching the earth surface, being absorbed by them, conversely to UVA and UVB that consequently, depending on their skin penetration potential, higher for UVA, are harmful for the skin. As a result, UVA radiations can reach dermis and alter collagen and elastin fibers structure, thus causing premature skin aging and promoting the onset of other skin diseases.(Rünger, 1999; Serpone et al., 2007) UVB radiations, instead, interest the most superficial layer of the skin, the epidermis, provoking sunburn, erythema and other skin diseases.(Serpone et al., 2007) Skin defends itself by the UV radiations using antioxidants such as vitamins, but is not always enough therefore sunscreens are required as additional protective barrier. Solar filters can be divided in two main classes: physical and chemical filters. In details, physical filters, also called inorganic filters, have shielding properties, being capable of reflecting the sun rays without being altered. Nowadays, the most used physical filters are zinc oxide (ZnO) and titanium dioxide (TiO_2).(Serpone et al., 2007) Chemical filters, also named organic filters, on the other hand, are usually aromatic compounds able to absorb the energy of UV radiation, releasing it as heat or radiation at higher wavelength.(Antoniou et al., 2008) Among chemical filters, the most used are benzophenones, octinoxate and avobenzone.(Jain & Jain, 2010) Despite organic filters are cheaper, more easily workable and favor more comfortable textures, some of them cannot absorb the UVA radiation and have been proven to increase the environment pollution, to be photo-instable, generating allergenicity, sensitization(Wang et al., 2010) and in some cases to permeate the skin

barrier damaging the endocrine system.(Hiller et al., 2019) For this reasons, inorganic filters, especially TiO_2, shielding the skin from both UVA and UVB radiation, are considered more attractive for sunscreens. However, also TiO_2 have some limitations regarding its size and it photoreactivity. Big particles, indeed, are unevenly included in the sunscreens, resulting in difficult spreading and causing whitening effect on the skin. On the other hand, small particles (nano-sized)(Monteiro-Riviere et al., 2011) despite improving sunscreen texture,(Shi et al., 2012) increase also the risk of skin deeper layers penetration, causing phototoxic reactions and skin irritations.(Schulz et al., 2002) Additionally, TiO_2 is known for its high photocatalytic activity, making possible the generation of reactive oxygen species (ROS), which can oxidize and degrade other ingredients in the formulation, raising safety concerns.(Shao & Schlossman, 1999; Tan et al., 1996) Finally, since sunscreen are mainly used on the beach, when they dissolve in water, also marine environment can be damaged by these nanoparticles, harming corals and accumulating in the food chain.

For all these reasons, the greater attention to the human health and environment protection has led, in recent years, to an increase in all the regulatory aspects concerning this sector, which are becoming more and more severe. As consequence, there is an urgent need for developing a safer but still effective sunscreen. This could be achieved by using biocompatible and non-toxic materials that do not permeate the skin barrier. In the last decade, there has been a growing interest in compounds containing calcium phosphates (CaPs), especially hydroxyapatite (HA), the main component of hard human connective tissues, for various applications, such as bone tissue engineering or drug delivery due to their excellent biocompatibility, biomimicry and non-toxicity.(Hossan et al., 2014)

A bioinspired in-lab biomineralization process, allowed to nucleate hydroxyapatite crystals directly on the organic matrix obtaining inorganic nano-metric particles confined and linked to the organic molecules resulting in nanostructured hybrid material.(Elisabetta Campodoni, Dozio, et al., 2020; Dellaquila et al., 2020; Krishnakumar et al., 2018; Anna Tampieri et al., 2008) In addition, HA lattice allows doping with foreign ions (like Mg^{2+}, Sr^{2+}, CO_3^{2-}, $Fe^{2+/3+}$, Ti^{4+}), thus making it a multifunctional tailored product.(E. Campodoni et al., 2016; Fernandes Patrício et al., 2021; Landi et al., 2006, 2007; Anna Tampieri et al., 2012) For all these promising features, HA have been already proposed as inorganic sunscreen agent.(Carella et al., 2021; Piccirillo et al., 2014)

With these evidences, this work aims to offer important innovations to the sector of cosmetic by investing in the design, development and validation of new eco-sustainable physical UV filters that can replace those currently in use whose safety is not fully well established. This work is focused on calcium-phosphate based biomimetic and hybrid particles with UV filtration behavior thanks to the HA multifunctionality. In detail, titanium-doped hydroxyapatite (TiHA) nucleated on two different organic sources, gelatin (Gel), animal-derived, and alginate (Alg), plant-derived, has been designed. The so developed bio-composites are classified as inorganic filters meeting the standard requirements imposed by current regulations. In fact, these particles are fully biodegradable in sea water, and their degradation products are not harmless, moreover they are devoid of photocatalytic potential so that, if after their use they end in coastal waters, they will not be responsible of marine ecosystems damaging, thus offering the opportunity of putting on the market eco-sustainable sunscreen products.

2. Materials&Methods

2.1. Synthesis process

2.1.1. Synthesis of titanium-doped hydroxyapatite biomineralized on gelatin (GelTiHA)

Preparation of TiHA nanocrystals, through heterogeneous nucleation on assembling gel matrix was carried out by means of a neutralization reaction performed as follow. A gelatin solution (3.32 g of gel in 83 mL H_2O at 45 °C) was mixed with a phosphate solution (3.46 g of H_3PO_4 in 30 mL H_2O) to obtain an acid solution. In the meantime, a solution of $Ti(iOPr)_4$ was prepared by adding 2.20 g of titanium in 15 mL of isopropanol under argon flux to avoid the oxidation of Ti4+. Finally, a basic solution was obtained dispersing 3.90 g of $Ca(OH)_2$ in 100 mL of H_2O at 45 °C under mechanical stirring for 30 minutes. The acid and titanium solution were then transferred separately in two cylindrical dropping funnels and slowly and simultaneously added dropwise to a neck round-bottom flask, where the basic solution at 45 °C under vigorous mechanical agitation was contained, paying attention to make them finish at the same time and avoiding $Ti(iOPr)_4$ oxidation by touching the flask before reaching the basic solution. During the dripping, it is possible to observe the solution turning increasingly white. Once finished the dripping, the suspension was kept under stirring under controlled temperature (45 °C) for 2 hours, and then left to rest without stirring and heating for 1 hour. At last, the product was centrifuged at 11000 rpm for 10 minutes, the pellet rinsed with double-distilled water for three times and then freeze-dried. A controlled freeze-drying process was applied, setting the cooling temperature at −40 °C and the heating ramp at 5 °C min^{-1} up to −5 °C and 2 °C min^{-1} up to 15 °C, under a pressure of 0.086 mbar until the obtainment of a dried powder.

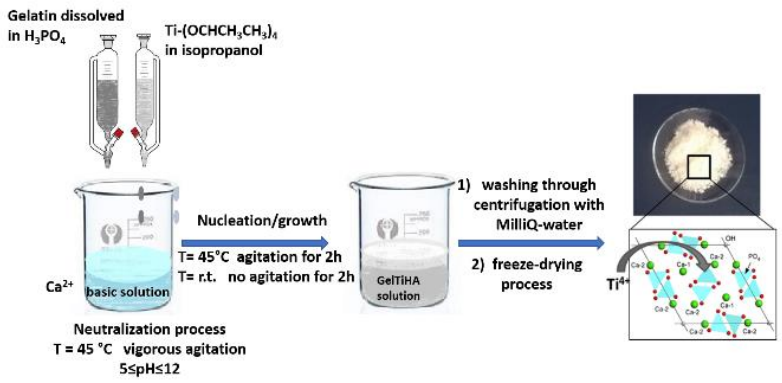

Figure 1. Schematic representation of GelTiHA synthesis

2.1.2. Synthesis of titanium-doped hydroxyapatite biomineralized on alginate (AlgTiHA)

Preparation of TiHA nanocrystals, through heterogeneous nucleation on assembling alginate matrix was carried out by means of a neutralization reaction performed as follow. A basic solution of $Ca(OH)_2$ (4.72 g of Ca(OH)2 in 100 mL H_2O) and a phosphate solution (4.15 g of H_3PO_4 in 30 mL H_2O) were prepared. In the meantime, a solution of $Ti(iOPr)_4$ was made by adding 1.90 g of titanium in 15 mL of isopropanol under argon flux to avoid the oxidation of Ti^{4+}. The basic solution was heated up to 45 °C under vigorous blades stirring for 30 minutes. Afterwards, the phosphate and titanium solution were transferred separately in two cylindrical dropping funnels and slowly and simultaneously added dropwise to the 45°C basic solution under vigorous mechanical stirring, paying attention to make them finish at the same time and avoiding $Ti(iOPr)_4$ oxidation by touching the flask before reaching the basic solution. During the dripping, it is possible to observe the solution turning increasingly white. Once finished the dripping, alginate solution (4 g of alginate in 100 ml H_2O) was slowly added to the mixture in order to avoid agglomerates formation. The suspension obtained was kept under stirring at controlled temperature (45 °C) for 2 hours, then left to rest without stirring and heating for 1 hour. Finally, the product was centrifuged at 11000 rpm for 10 minutes. The pellet obtained was rinsed with double-distilled water for three

times and then freeze-dried. A controlled freeze-drying process was applied setting the cooling temperature at −40 °C and the heating ramp at 5 °C min^{-1} up to −5 °C and 2 °C min^{-1} up to 15 °C under a pressure of 0.086 mbar until the obtainment of a dried powder.

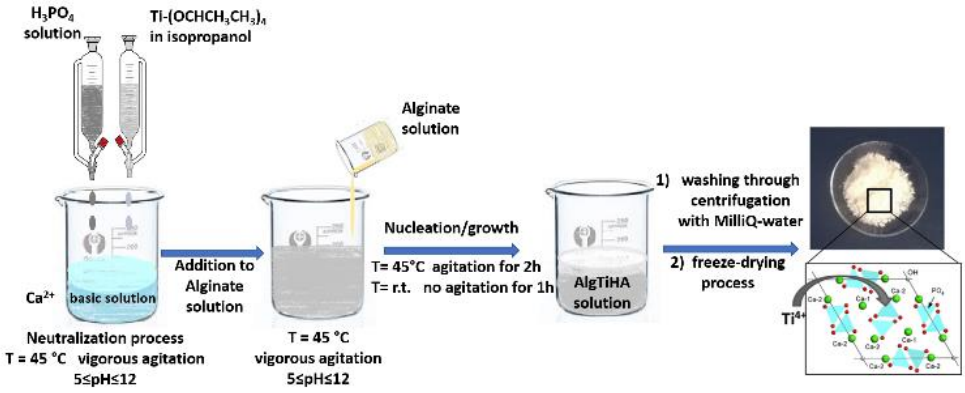

Figure 2. Schematic representation of AlgTiHA synthesis

2.2. Characterization methods

2.2.1. Scanning Electron Microscopy (SEM)

The samples morphology was examined by scanning electron microscopy (SEM). In particular, the equipment employed were a FEG-SEM (Field Emission Gun Scanning Electron Microscope, FEI, Quanta 200, USA) for high resolution images at high magnification and ESEM (Environmental Scanning Electron Microscope, Quanta 600 FEG, FEI Company, Hillsboro, OR) for high resolution images at low magnification. For both the analysis, the specimens were previously mounted on aluminum stubs by means of carbon tape and gold coated using a coating units Polaron Sputter Coater E5100 (Polaron Equipment, Watford, Hertfordshire, UK). The dimensional analysis was performed by means of ImageJ software.

2.2.2. X-Ray Diffraction (XRD)

The crystal structure of the composites was established by powder XRD analysis. The D8 Advance diffractometer model (Bruker, Karlsruhe, Germany) working with Bragg-Brentano configuration was employed, equipped with a LINXEYE position-sensitive detector (CuKα radiation, λ=1.5418Å) generated at 40 kV and 40 mA. The XRD patterns were recorded in the 2θ range 10°-80°, scan step 0.02° and step time 0.5 seconds.

2.2.3. Thermogravimetric analysis (TGA)

The thermal behavior of the composites was determined using the Simultaneous Thermal Analyzer (STA 409C, Netsch, Germany). The experiment was carried out in the temperature range of 10-1100 °C using a heating rate of 10 K/min in air flow. For the analysis, 20 mg of sample and Al_2O_3 crucible were employed.

2.2.4. Fourier-Transform Infrared Spectroscopy (FTIR)

The spectra were collected by a Thermo Nicolet-Avatar 320 FT-IR (Thermo Fisher Scientific Inc., Waltham, MA, USA). For the analysis about 2 mg of the sample were finely ground with 100 mg of anhydrous potassium bromide (KBr) in order to remove scattering effects from large crystals, and then pressed at 8000 psi into 7 mm diameter disc to form a translucent pellet. All the spectra are the average of 64 spectra, collected at room temperature in the wavelength range of 400-4000 cm-1 at a resolution of 4 cm-1. Potassium bromide was used as control.

2.2.5. Inductive Coupled Plasma Optical Emission Spectroscopy (ICP-OES)

To perform the analysis an ICP-OES Liberty 200, Varian (Clayton South, Australia) was employed. Samples were prepared by dissolving 20 mg of each in 2 mL of nitric acid (HNO_3) and then making them up to 100 mL volume with deionized water after 30 minutes' sonication. Standard solutions of the element of interest were used as reference and an equally diluted solution of nitric acid as blank.

2.2.6. Ultraviolet/Visible Spectroscopy

A UV-Vis-NIR spectrophotometer Lambda 750, (Perkin Elmer Instrument, USA) was used to perform absorbance measurements. The powders were suspended in distilled water with a concentration of 10 mg L-1 and sonicated for 10 minutes with a sonicating probe. The absorbance spectra of the AlgTiHA and GelTiHA were recorded from 250 to 700 nm and compared with the ones of the commercial powder Solaveil. The same spectrophotometer was used to analyze the reflection properties of the samples. The powders were loaded on a sample holder and the spectrum was recorded from 280 nm to 780 nm.

2.2.7. Photodegradation test

Photodegradation tests were carried out for each synthesized powder to evaluate the samples ability to degrade Rhodamine B (≥95%, Sigma Aldrich) under a simulated sunlight. 50 mg of powder was loaded in a refrigerated becker with 60 mL of rhodamine B solution 5 mg L^{-1}. The powder was stirred in dark for 30 minutes to allow the absorption of Rhodamine B molecule on the powder surface. At the end of the dark period, the refrigerated becker was irradiated with a solar simulator (ABET Technologies Sun 2000, Connecticut), previously calibrated with a Silicon reference cell at 1000 W m2 AM 1.5; 3 mL of suspension were analyzed at the UV-Vis-NIR spectrophotometer at specific times (0, 15, 30, 60, 90 and 120 minutes) after a centrifugation at 5000 rpm for 1 minute to separate the powder from the dye solution.

2.2.8. Cell culture

BALB/3T3 murine fibroblast (Clone A31, ATCC® CCL-163™) were cultured in high glucose with pyruvate Dulbecco's Modified Eagle's Medium (DMEM) (Gibco) supplemented with 10% Calf Bovine Serum (CBS, Gibco) and 1% penicillin-streptomycin solution (100 U/ml-100 µg/mL, Gibco) and kept at 37 °C under 5% CO_2 atmosphere conditions and controlled humidity. Cells

were detached from culture flask by trypsinization and centrifuged. The cell number and viability were defined by Trypan Blue Dye Exclusion test.

AlgTiHA, GelTiHA and Solaveil disk were obtained pressing 0.5 g each with final dimension of 15 × 2 mm Ø x h (60 seconds at 110 mbar, CCR Nannetti, A/84) and they were sterilized by 25 kGy gamma-ray radiation prior to use. They were pre-conditioned for 24 hours in complete culture media before seeding 80.000 cells/sample by carefully dropping 30 µl cell suspension on the sample upper surface. After 30 minutes-incubation at 37 °C that allows a preliminary cell adhesion, 1.5 ml of complete culture media was added to each sample and gently changed after 3 days. Cell cultures were kept at 37 °C with 5% CO_2 atmosphere and controlled humidity conditions up to 7 days. All cell-handling procedures were performed under biological laminar-flow hood and sterility conditions.

2.2.9. Cell viability analysis

Quantitative cell viability analysis was performed via MTT assay. Briefly, MTT reagent ([3-(4,5-dimethylthiazol-2-yl)-2,5-diphenyltetrazolium bromide] (Sigma) was dissolved in Phosphate Saline Buffer 1X (PBS 1X) (5 mg/mL). At each time point of culture (1, 3 and 7 days), the samples were incubated with 10% well-volume MTT solution for 2 hours at 37 °C. The culture medium was then removed and substituted by Dimethyl Sulfoxide (DMSO), which dissolves insoluble formazan crystals derived from MTT conversion by metabolism of live cells. After 15 minutes' incubation under slight stirring conditions, each supernatant was transferred to a 96 well-plate in triplicate (200 µL/well) and the absorbance was read at 570 nm by Multiskan FC Microplate Photometer (Thermo Scientific). The values of absorbance were directly proportional to the number of live cells. For each type of material, three samples were analyzed at each time point.

Qualitative cell viability and cytotoxicity analysis of the samples was performed via Live/Dead Assay for its ability to discriminate live from dead cells by simultaneously staining the esterase activity and the loss of plasma membrane integrity, respectively. At day 1 of culture, Live/Dead Assay Kit (Invitrogen) was performed according to manufacturer's instructions. In brief, the samples were washed in PBS 1X and incubated in Live/Dead solution composed by PBS 1X, Acetoxymethyl Calcein (AM-calcein) 2 μM and Ethidium homodimer-1 (EthD-1) 4 μM for 15 minutes at 37 °C in dark conditions. Samples were washed and rinsed in PBS 1X. The image acquisition was performed by an inverted Ti-E fluorescence microscope (Nikon). For each type of material, one sample was analyzed.

2.2.10. Cell morphology evaluation

Qualitative fluorescent detection of cell actin filaments and nuclei was performed at day 3 of culture. Samples were washed in PBS 1X and fixed in 4% (w/v) paraformaldehyde (PFA) (Sigma) for 15 minutes. The samples were then permeabilized in PBS 1X with 0.1% (v/v) Triton X-100 for 15 minutes at room temperature, and incubated with FITC-conjugated fluorescein-phalloidin (38 nM, Invitrogen).(Faulstich et al., 1988) Samples were washed with PBS 1X for 5 min and incubated with nuclear stain 4'-6-Diamidino-2-phenylindole (DAPI) (Invitrogen) 300 nM in PBS 1X per 5 min. The images were acquired by inverted Ti-E fluorescence microscope (Nikon). For each type of material, one sample was analyzed.

A further evaluation of cell morphology and cell-material interaction was performed by Scanning Electron Microscope (SEM) analysis at day 3 of culture. Briefly, the samples were washed in 0.1 M Sodium Cacodylate Buffer pH 7.4 and fixed in 2.5% Glutaraldehyde (Sigma) in 0.1 M Sodium Cacodylate Buffer pH 7.4 for 2 hours at 4°C. After washings in 0.1 M Sodium Cacodylate Buffer pH 7.4, the samples were dehydrated in a graded series of ethanol followed by

Hexamethyldisilazane reagent (HMDS ≥ 99%, Sigma). For the analysis, the samples were sputter-coated with 20 μm of gold film. For each type of material, one sample was analyzed under high vacuum conditions by SEM (ESEM Quanta 200, FEI).

2.2.11. Statistical Analysis

Statistical analysis of MTT data was performed by GraphPad Prism software (version 6.0). The results were reported in the graph as mean ± standard error of the mean and they were analyzed by two-way analysis of variance (two-way ANOVA) followed by Dunnett's multiple comparison test compared to Solaveil control.

3. Results&discussion

The direct nucleation of Ti-doped HA nanocrystals onto polymeric matrices occurred by an in-lab biomineralization reaction in which polymers have strictly controlled various steps of the process like the nucleation, crystallization, growth and even morphology of hydroxyapatite particles, mainly playing a role of crystallization inhibitors.

Exactly as it happens in the in-lab biomineralization of collagen,(Elisabetta Campodoni et al., 2021; Krishnakumar et al., 2017; C. Menale et al., 2019; Anna Tampieri et al., 2008) gelatin molecules promote the heterogeneous nucleation of low crystalline hydroxyapatite nanoparticles through a neutralization method. For the obtainment of GelTiHA, the reaction was performed by first mixing together the phosphoric acid and gelatin solutions to then dripping them into the alkaline calcium hydroxide suspension contemporarily with the titanium solution. The pH of the suspension was decreased up to neutral value, at which the mineral nucleation happens thanks to the calcium ions binding operated by the carboxylic groups exposed by gelatin molecule. Differently, for AlgTiHA, alginate need to be introduced after the neutralization process is concluded, since both acid and basic environments induce alginate gelation.(Yotsuyanagi et al.,

1991) For this reason, the alginate solution was poured immediately after dropping the phosphoric acid solution in the alkaline calcium hydroxide suspension, at the same time of the titanium solution.

Both the hybrid particles, obtained through a bio-inspired process, were compared with one of the most employed commercial UV filter, with the aim to highlight how these materials can suitably replace the commercial ones, maintaining and improving the reflectance properties without showing any toxicity for humans as well as for the marine environment. (Adamiano et al., 2017)

In contrast to collagen, one of the biopolymers best known for promoting the biomineralization process, and which tends to assemble during the process forming three-dimensional fibrous structures, Gel and Alg are apt to promote the nucleation of HA but without their spontaneous self-assembly, resulting in mineralized disaggregated hybrid particles formation featured by high percentage of mineral phase. This, also favored from the involvement of most of their functional groups in the interaction with calcium and phosphate ions, that increase the mineralization rate preventing the formation of three-dimensional structures.(Elisabetta Campodoni et al., 2021; Elisabetta Campodoni, Montanari, et al., 2020; Landi et al., 2008; Ciro Menale et al., 2018; Shankar et al., 2017; A Tampieri et al., 2011) The hybrid particles morphology is clearly visible through SEM-FEG (Figure 3); both GelTiHA and AlgTiHA samples consists of needle-like particles of, respectively, 304 ± 55 nm and 267 ± 76 nm length (n=30), with a slightly higher tendency to aggregate of the AlgTiHA particles.

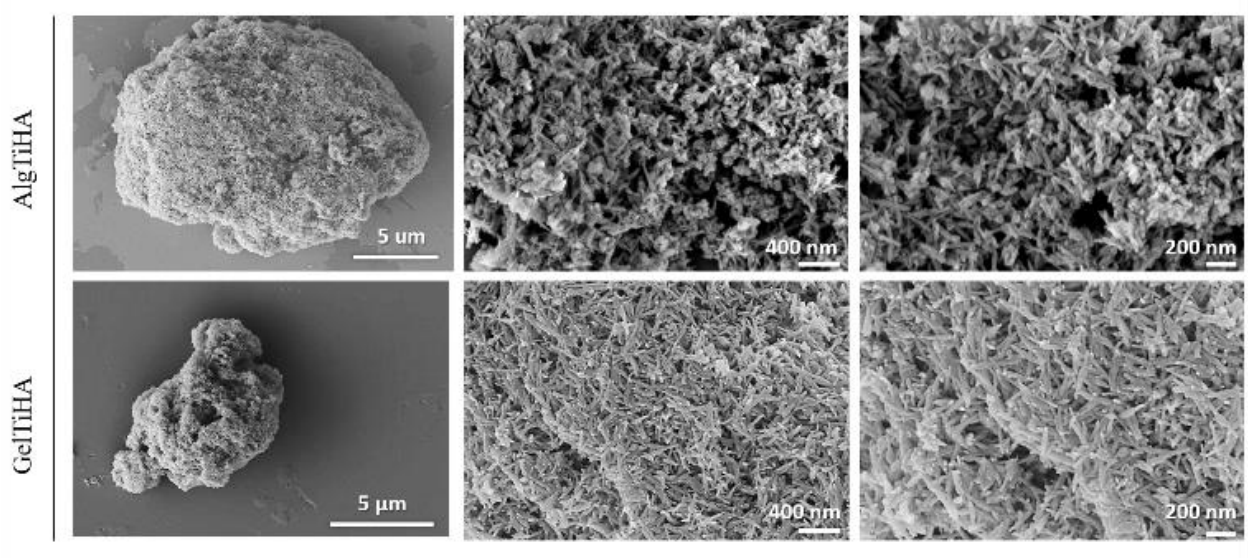

Figure 3. SEM-FEG images of AlgTiHA and GelTiHA hybrid composites

It is true that in literature, is reported that the needle-like shape of particles might induce the production of inflammatory cytokines, which in turn determine a different cytotoxicity of the material. In particular, the needle-shape would present a potential toxicity for cells, as it is able to break the cell membrane and lead to their death.(Zhao et al., 2013) Nevertheless, from a recent document issued by the Scientific Committee on Consumer Safety(European Commission, 2021) it has also made clear that the rod-shape of particles is the most suitable for cosmetic use, since it is less dangerous for the skin. SCCS claimed to be ready to assess any evidence provided to support safe use of the materials in cosmetic products. It must be highlighted though, that both AlgTiHA and GelTiHA, despite the needle-like form, are not inorganic single dispersed particles, but are hybrid materials, with the inorganic phase strictly linked and interconnected with the organic matrix, which forces them to clump together potentially limiting their penetration into the dermis and a possible toxic effect. This test would be part of a more complex dossier to be presented to SCCS supporting the safe use of hydroxyapatite mineralized on organic matrix in cosmetic products.(European Commission, 2021)

As mentioned above, the mineralization of Gel and Alg matrix allowed to obtain a high mineral content confirmed by thermogravimetric analysis (TGA) that assess the weight loss % by at each temperature range, giving information on composites composition: content of water, organic fraction and mineral fraction (Figure 4). TGA profiles revealed two different weight loss, the first, ranging from 20 °C to 150 °C, consisting in water loss, whereas the second, ranges from 150 °C to 800 °C, consisting in polymer degradation in line with literature reported.(Kuzema et al., 2015; Soares et al., 2004; A. Tampieri et al., 2005) The residual mass corresponds to the mineral component, TiHA, which has been biomineralized on biopolymers. In detail, Gel:TiHA ratio is more similar to the theoretical ratio (20:80), while the one of Alg:TiHA is lower than 20:80, showing that less organic phase is present. This behavior can be ascribable to the different biomineralization protocol (Alg was introduced after neutralization process) and to the high affinity between Ca^{2+} ions and Alg, which favour the immediate interaction between the just formed hydroxyapatite and the alginate poured.

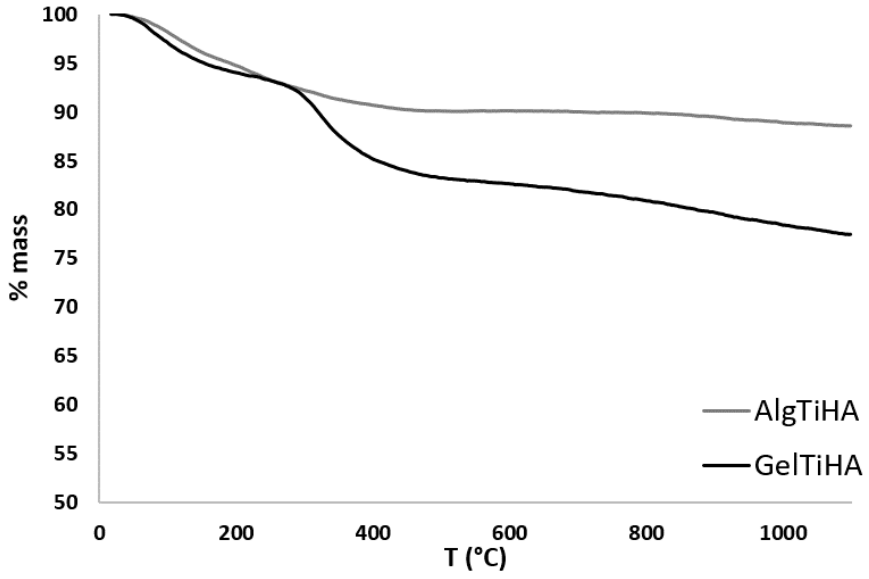

Figure 4. Thermal decomposition profile (TGA) of AlgTiHA and GelTiHA

XRD profiles showed the presence of a pure crystalline phase that can be identified as apatitic structure according to the PDF cards #09-0432 (Figure 5A). Both XRD patterns are poorly resolved and with low intensity, typical of mineral phases with a low degree of crystallinity. The scarce crystallinity may be ascribed to various factors, firstly, the low synthesis temperature does not allow an atomic rearrangement in favour of more crystalline structures, which are thermodynamically more stable. Furthermore, the presence of biopolymers (gelatin and alginate) directs the mineralization towards the formation of low crystallinity mineral phases, typical of the biomineralization processes, in which the organic molecules act as a template for the nucleation of the mineral phase, and as an obstacle for its growth.(Elisabetta Campodoni, Dozio, et al., 2020; Anna Tampieri et al., 2008) Finally, the presence of titanium ions during the crystal lattice formation, has the effect of distorting the lattice itself, thus leading to an increase in disorderly areas and causing the formation of poorly crystalline phase. No secondary crystalline phases are identified (e.g. TiO_2), highlighting as Ti ions are present inside the HA lattice or could be present as secondary, but highly amorphous, phase not detectable to the XRD nor visible to SEM.(Adamiano et al., 2017)

Among spectroscopy techniques, Infrared spectroscopy (FTIR) deals with the region of the electromagnetic spectrum ranging from 4000 to 400 cm-1 (from near to far-IR). FTIR analysis of GelTiHA and AlgTiHA revealed a similar pattern (Figure 5B) showing peaks at 1036, 602, 562 cm-1. The signal at 1036 cm^{-1} corresponds to the asymmetric stretching of PO_4 groups of HA, while, peaks at 602 and 562 cm^{-1} are related to the bending of the PO_4 group of the HA.(Shankar et al., 2017) In AlgTiHA, only peaks related to the mineral phase are clearly visible probably due to the very high amount of hydroxyapatite fully covering the Alg molecules. Quite the opposite, in GelTiHA where a major amount of organic phase is present, also Gel peaks are clearly visible.

In particular, the peak at 3405 cm^{-1} corresponds to the stretching vibrations of O-H bonds of Gel, while the peaks at 1650, 1547 and 1453 cm^{-1}, are related to the asymmetric and symmetric stretching vibrations of the carboxylate groups in Gel.(Elisabetta Campodoni, Montanari, et al., 2020; Shankar et al., 2017)

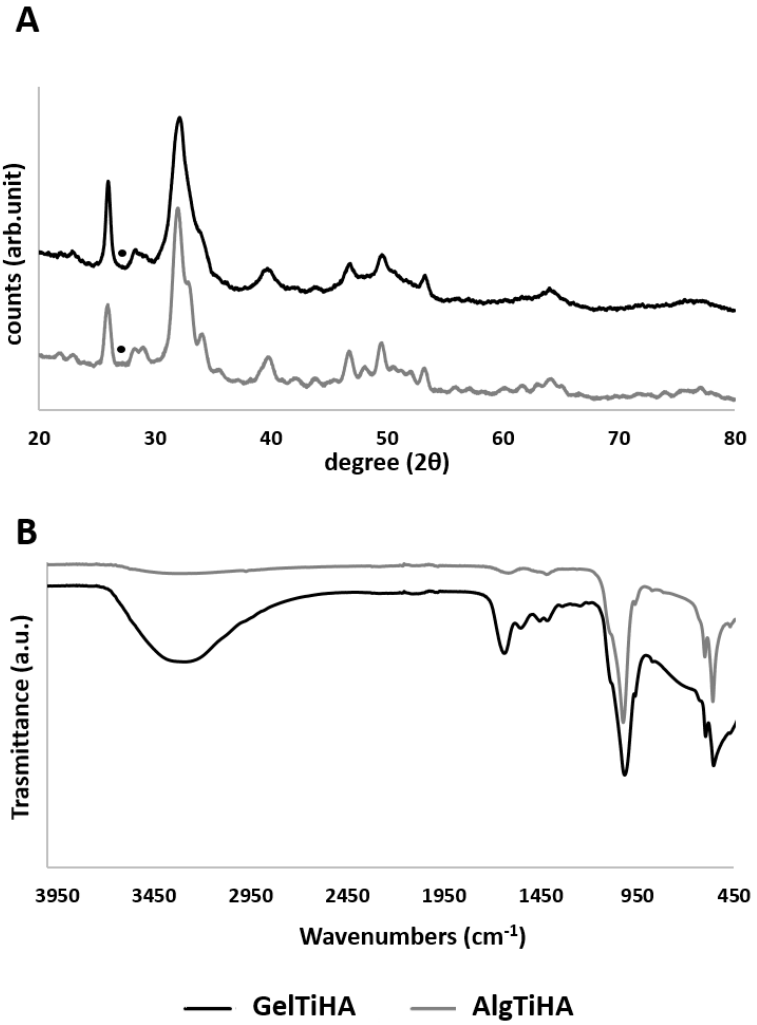

Figure 5. A) XRD spectra and B) FTIR spectra of AlgTiHA and GelTiHA hybrid composites. Black dots refer to TiO2 highest intensity peak

The chemical composition of the mineral phase was measured by ICP quantitative analyses in terms of molar ratio between the elements (Table 1). Considering the evidences highlighted from XRD analyses it was possible to assess the effective partial substitution of both Ca^{2+} ions and PO_4^{3-}

ions in the HA lattice by, respectively, Ti^{4+} and TiO_4^{4-} ions, coherently with what previously reported in literature.(Adamiano et al., 2017) In particular, as expected, an increment of the (Ca + Ti) / P value compared to the Ca / P value was recorded, as well as a decrease in the Ca / (Ti + P) value. The small deviation of the Ca / P values from that of the pure HA (theoretical ratio 1.67) can plausibly be attributed to a similar Ca^{2+} and PO_4^{3-} ions depletion by Ti^{4+} and TiO_4^{4-} ions.

Table 1. Inorganic/organic ratio and chemical composition of GelTiHA and AlgTiHA evaluated by TGA and ICP

	HA:Pol ratio	Ca/P (mol)	Ti/Ca (mol)	Ti/P (mol)	Ca/(Ti+P) (mol)	(Ca+Ti)/P (mol)	(Ca+Ti)/(P+Ti) (mol)
GelTiHA	84:16	1,66 ± 0.01	0,15 ± 0.01	0,25 ± 0.01	1,33 ± 0.01	1,91 ± 0.01	1.53 ± 0.01
AlgTiHA	92:8	1,60 ± 0.03	0,14 ± 0.01	0,23 ± 0.01	1,30 ± 0.04	1,84 ± 0.01	1.49 ± 0.03

The UV-Vis spectroscopy is the best technique to determinate the absorption and reflection properties of sunscreen composites. The reflection properties of the hybrid composites were reported in figure 6A. The reflectance profiles of both composites were very similar, GelTiHA and AlgTiHA revealed an area of middle values of reflectance between 280 and 320 nm followed by an increase of the reflectance value in the UVA range (315-400 nm) reaching a plateau of 90% of reflectance at the edge of the visible range (400 nm). Comparing the reflection curves of the hybrid composites with a commercial sunscreen, it is clear how the reflectance values in the UVA and UVB (315-400 nm and 280-315 nm) range of Solaveil (TiO_2 based commercial sunscreen) is

significantly lower (10%) than GelTiHA and AlgTiHA, confirming even more the good reflection properties of these hybrid composites.

On the other hand, GelTiHA and AlgTiHA show lower absorption (figure 6B) than the commercial product: the curves decrease in almost linear manner with the wavelength, while Solaveil presents an enhanced absorption, with a maximum peak at 350 nm to then decrease such as GelTiHA and AlgTiHA. In conclusion, both hybrid composites have excellent reflectance properties in the UVA range and can reflect the radiation also in UVB range. These properties make GelTiHA and AlgTiHA efficient physical filters for sunscreen composition.(Piccirillo et al., 2014; Smaoui et al., 2017)

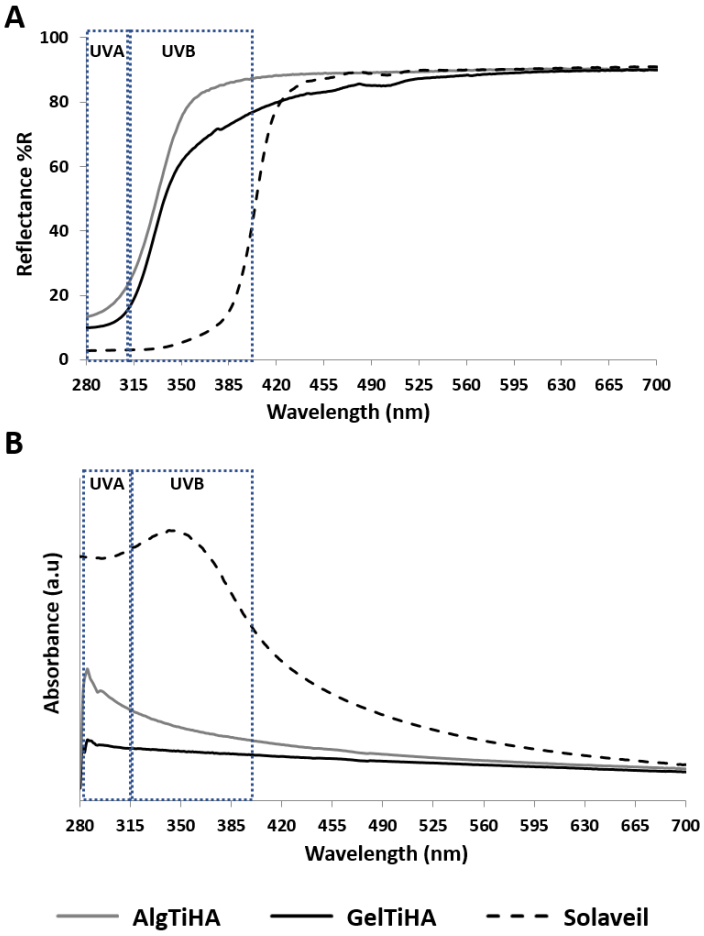

Figure 6. A) Reflectance spectra and B) Absorption spectra of AlgTiHA and GelTiHA hybrid composites in comparison with a commercial standard.

Finally, photodegradation tests of an aqueous solution of Rhodamine B were carried out exposing the system under a simulated full solar spectrum. No photocatalytic activity was detected by either AlgTiHA and GelTiHA, sign there is no formation of radicals and/or reactive species under irradiation and highlighting their potential as innovation for sunscreens. On the contrary, the commercial sunscreen Solaveil, showed photocatalytic activity, visible by the decrease of the Rhodamine B maximum absorption during the solar simulator

time exposure. More than 50% of Rhodamine B was degraded in 120 minutes (Figure 7).

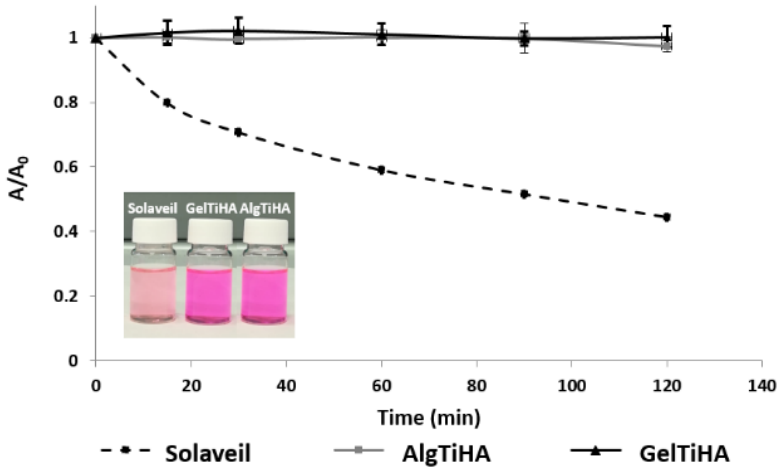

Figure 7. Photodegradation of AlgTiHA and GelTiHA in comparison with a commercial standard. Picture on the right show samples after photodegradation test. Insert: picture of Solaveil, GelTiHA and AlgTiHA solutions after solar irradiation.

To assess the safety of the samples, in vitro biological test was performed with fibroblast cells thus to analyze the biocompatibility of AlgTiHA and GelTiHA compared to the commercial

control Solaveil. Quantitative cell viability analysis by MTT assay clearly showed higher viability of cells grown on both TiHA-based sunscreens during the whole experiment, demonstrating the absence of cytotoxic effect. In detail, figure 8 showed statistically significant increase of proliferation of AlgTiHA (p values ≤ 0.05) and GelTiHA (p values ≤ 0.0001) samples at day 4 and 7 of culture, respectively, compared to Solaveil. In addition, GelTiHA sunscreen showed a linear cell culture growth, while AlgTiHA halted the cell proliferation and no differences in cell viability were seen between day 4 and day 7 of culture (Figure 8).

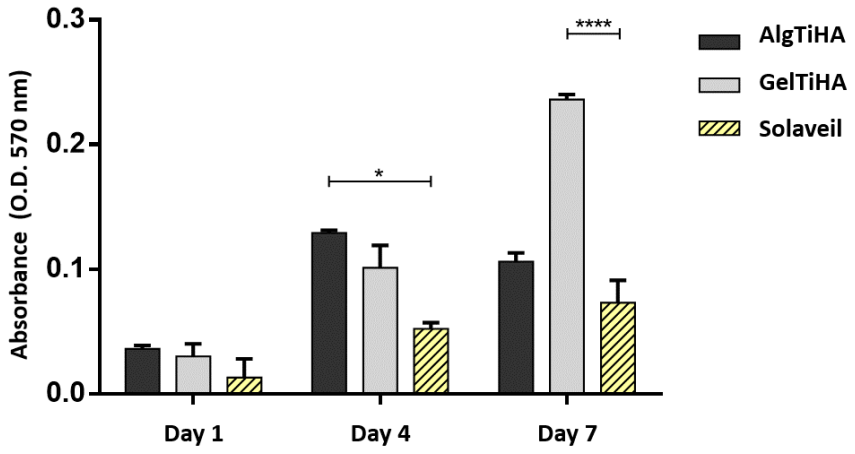

Figure 8. Cell viability analysis by the MTT test. The results were reported in the graph as mean ± error standard of the mean; *p value ≤ 0.05 and **** p value ≤ 0.0001

The absence of cytotoxicity was also confirmed by a qualitative cell viability analysis performed with Live/Dead assay. In fact, both GelTiHA and AlgTiHA samples did not compromise the cell viability. At day 1, several live cells and very few dead cells were detected in both groups compared to the control group that showed a higher cytotoxicity (Figure 9, panel A, B and C). It is important to notice that, 24 hours after seeding, GelTiHA group showed also a more uniform cell distribution on the sample surface compared to the other two groups (Figure 9, panel A, B and

C). This ability of the cells to adhere to the sample is related to the biocompatibility of the material itself. In detail, cell/surface interaction and cell adhesion are complex processes involving the reorganization of cytoskeleton proteins like actin (Anselme, 2000). In figure 9 (panel D, E and F) phalloidin stains actin filaments and a cell layer that covers the sample surface is evident in GelTiHA and AlgTiHA groups. Instead, the control group showed very few cells with irregular morphology confirming the qualitative and quantitative data of cell viability.

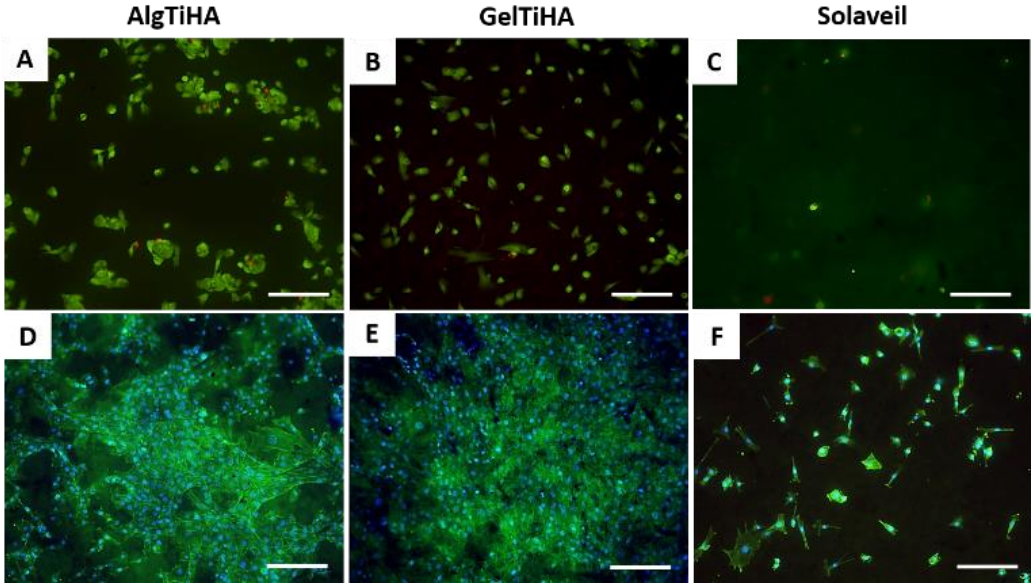

Figure 9. A, B and C) Live/Dead Assay at day 1. Calcein stains live cells in green and Ethidium homodimer-1 stains dead cells in red; D, E and F) Cell morphology analysis at day 3. Fluorescein-phalloidin detection of actin filaments in green and DAPI detection of nuclei in blue. Scale bars 200 μm

A further evaluation of cell morphology and interactions with the samples was also reported by SEM analysis at day 3 (Figure 10). The SEM images confirmed the results detected with actin staining: both AlgTiHA and GelTiHA were favorable to cell adhesion and a higher cell density is present compared to the control group. The different compositions of the hybrid composite

samples positively affect the cell behavior respect to the commercial Solaveil (Figure 10, panel A-F).

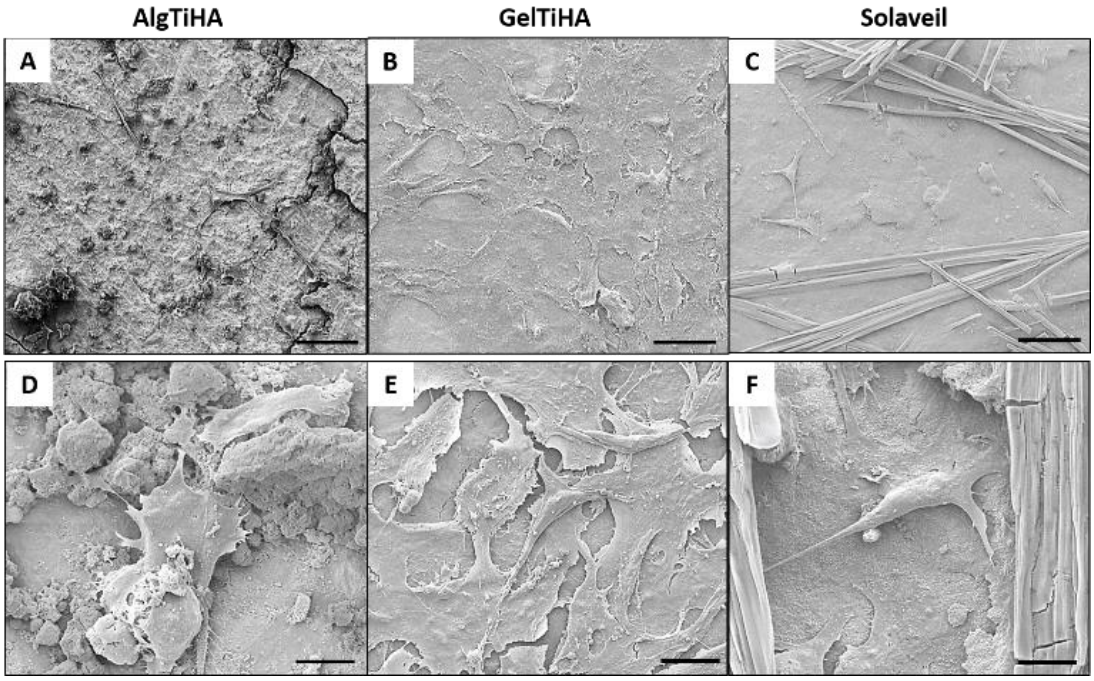

Figure 10. SEM images of fibroblast cells grown in contact with the AlgTiHA (A, D), GelTiHA (B, E), Solaveil (C, F) at day 3 of culture. Scale bars 100 μm (A, B, C) and 20 μm (D, E, F)

4. Conclusion

Within this work, we reported the unique employment of our previously developed and reported in-lab biomineralization process for the creation of innovative hybrid phases useful as UV physical filters for the production of eco-sustainable sunscreen formulations.

More specifically, two distinct hybrid composites (GelTiHA and AlgTiHA) based on Ti-doped hydroxyapatite, were successfully developed demonstrating to be effective as UV filters and, because of their CaP-based composition, highly safe for human and for the environment in comparison to ZnO and TiO_2 nowadays commonly used as mineral filters. The introduction of Ti ions during the biomineralization process, allowed to obtain the partial substitution of both Ca^{2+}

(with Ti^{4+}) and PO_4^{4-} (TiO_4^{4-}) ions into the hydroxyapatite latex realizing innovative physical solar filters featured by high biocompatibility, and UV radiations absorption/reflection bands in the desired range. In addition, despite the nanometric size of the particles, the organic matrix, naturally non-toxic for the skin, ensure their safety thanks to the close structural bond formed with the inorganic component, reducing their potential possible skin penetration ability. Finally, thanks to the presence of Ti ions as active component in place of TiO_2, zero photocatalytic effect was observed, with a consequent reduction of the risk of sensitization during sun exposure and giving the opportunity to develop sunscreen products with improved safety and eco-sustainability.

Author Contributions

Elisabetta Campodoni: Conceptualization, performed the experiments, writing original draft, read and approved the final manuscript. Margherita Montanari: performed the experiment, writing original draft, read and approved the final manuscript. Chiara Artusi: performed the experiment, writing original draft, read and approved the final manuscript. Linda Bergamini: Performed the UV-vis spectroscopy and photodegradation experiment writing original draft, read and approved the final manuscript. Giada Bassi: performed the biological experiments, writing original draft, read and approved the final manuscript. Silvia Panseri: Conceptualized the biological experiments, read and approved the final manuscript. Alessandra Sanson: read and approved the final manuscript. Anna Tampieri: read and approved the final manuscript. Monica Sandri: methodology, conceptualization, revised and approved the final manuscript.

Funding Sources

This project has received funding from the Project PoC2020-ProtecTHA “Innovative UV filters for safer and more eco-sustainable sun protection” Co-financed form MiSE and CNR.

References

[1] C. Antoniou, M.G. Kosmadaki, A.J. Stratigos, A.D. Katsambas, Sunscreens – what's important to know, J. Eur. Acad. Dermatology Venereol. 22 (2008) 1110–1119. doi:https://doi.org/10.1111/j.1468-3083.2007.02580.x.

[2] M. Battistin, V. Dissette, A. Bonetto, E. Durini, S. Manfredini, A. Marcomini, E. Casagrande, A. Brunetta, P. Ziosi, S. Molesini, R. Gavioli, F. Nicoli, S. Vertuani, A. Baldisserotto, A New Approach to UV Protection by Direct Surface Functionalization of TiO2 with the Antioxidant Polyphenol Dihydroxyphenyl Benzimidazole Carboxylic Acid, Nanomaterials. 10(2) (2020) 231. doi:10.3390/nano10020231.

[3] M.E. Burnett, J.Y. Hu, S.Q. Wang, Sunscreens: Obtaining adequate photoprotection, Dermatol. Ther. 25 (2012) 244–251. doi:10.1111/j.1529-8019.2012.01503.x.

[4] F. Yu, W. Ruoyu, Y. Lei, X. Lidan, H. Junfei, T. Jie, H. Hailun, G. Zhipeng, L. Yiwen, Propolis inspired sunscreens for efficient UV-protection and skin barrier maintenance, Nano Res. 15 (2022) 8237–8246. doi:10.1007/s12274-022-4434-z.

[5] Regulation (EC) No 1223/2009 of the European Parliament and of the Council of 20 November 2009 on Cosmetic Products., (n.d.). https://eur-lex.europa.eu/eli/reg/2009/1223 (accessed February 27, 2023).

[6] A.N. Barone, C.E. Hayes, J.J. Kerr, R.C. Lee, D.B. Flaherty, Acute toxicity testing of TiO2-based vs. oxybenzone-based sunscreens on clownfish (Amphiprion ocellaris), Environ. Sci. Pollut. Res. 26 (2019) 14513–14520. doi:10.1007/s11356-019-04769-z.

[7] S.L. Schneider, H.W. Lim, Review of environmental effects of oxybenzone and other sunscreen active ingredients, J. Am. Acad. Dermatol. 80 (2019) 266–271. doi:10.1016/j.jaad.2018.06.033.

[8] Y. Huang, J.C.F. Law, T.K. Lam, K.S.Y. Leung, Risks of organic UV filters: a review of environmental and human health concern studies, Sci. Total Environ. 755 (2021) 142486. doi:10.1016/j.scitotenv.2020.142486.

[9] S. Narla, H.W. Lim, Sunscreen: FDA regulation, and environmental and health impact,

Photochem. Photobiol. Sci. 19 (2020) 66–70. doi:10.1039/c9pp00366e.

[10] T. Manasfi, B. Coulomb, S. Ravier, J.-L. Boudenne, Degradation of Organic UV filters in Chlorinated Seawater Swimming Pools: Transformation Pathways and Bromoform Formation, Environ. Sci. Technol. 51 (2017) 13580–13591. doi:10.1021/acs.est.7b02624.

[11] G. Tortini, P. Ziosi, E. Cesa, S. Molesini, E. Baldini, D. De Lucia, C. Rossi, E. Durini, S. Vertuani, S. Manfredini, Criticisms in the Development of High-Protection and Broad-Spectrum "Natural/Organic" Certifiable Sunscreen, Cosmetics. 9 (2022) 56. doi:10.3390/cosmetics9030056.

[12] M. Vieira Sanches, M. Oliva, L. De Marchi, A. Cuccaro, D. Puppi, F. Chiellini, R. Freitas, C. Pretti, Ecotoxicological screening of UV-filters using a battery of marine bioassays, Environ. Pollut. 290 (2021) 118011. doi:10.1016/J.ENVPOL.2021.118011.

[13] COSMOS-standard AISBL, COSMOS Position on the Mineral UV-filter in Organic and Natural Cosmetics, (2020). https://media.cosmosstandard. org/filer_public/30/ea/30ea5944-cf28-44ab-bec6-f4f7ca6c74f1/cosmosstandard_ v31.pdf (accessed February 27, 2023).

[14] P.E. Bernauer U, Bodin L, Chaudhry Q, CoenraadsPJ, Dusinska M, Ezendam J, Gaffet E, Galli CL, Granum B, Octocrylene, (n.d.). https://health.ec.europa.eu/publications/octocrylene_en (accessed February 27, 2023).

[15] S.W.Y. Wong, G.J. Zhou, P.T.Y. Leung, J. Han, J.S. Lee, K.W.H. Kwok, K.M.Y. Leung, Sunscreens containing zinc oxide nanoparticles can trigger oxidative stress and toxicity to the marine copepod Tigriopus japonicus, Mar. Pollut. Bull. 154 (2020) 111078. doi:10.1016/j.marpolbul.2020.111078.

[16] N. Serpone, D. Dondi, A. Albini, Inorganic and organic UV filters: Their role and efficacy in sunscreens and suncare products, Inorganica Chim. Acta. 360 (2007) 794–802. doi:10.1016/j.ica.2005.12.057.

[17] N. Serpone, Sunscreens and their usefulness: have we made any progress in the last two decades?, Photochem. Photobiol. Sci. 20 (2021) 189–244. doi:10.1007/s43630-021-00013-1.

[18] P.J. Lu, S.W. Fang, W.L. Cheng, S.C. Huang, M.C. Huang, H.F. Cheng, Characterization of titanium dioxide and zinc oxide nanoparticles in sunscreen powder by comparing different measurement methods, J. Food Drug Anal. 26 (2018) 1192–1200. doi:10.1016/j.jfda.2018.01.010.

[19] D. Hanigan, L. Truong, J. Schoepf, T. Nosaka, A. Mulchandani, R.L. Tanguay, P. Westerhoff, Trade-offs in ecosystem impacts from nanomaterial versus organic chemical ultraviolet filters in sunscreens, Water Res. 139 (2018) 281–290. doi:10.1016/j.watres.2018.03.062.

[20] L. Tiano, T. Armeni, E. Venditti, G. Barucca, L. Mincarelli, E. Damiani, Modified TiO2 particles differentially affect human skin fibroblasts exposed to UVA light, Free Radic. Biol. Med. 49 (2010) 408–415. doi:10.1016/j.freeradbiomed.2010.04.032.

[21] F. Carella, L. Degli Esposti, A. Adamiano, M. Iafisco, The Use of Calcium Phosphates inCosmetics, State of the Art and Future Perspectives, Materials (Basel). 14 (2021) 6398. doi:10.3390/ma14216398.

[22] D.L. Slomberg, R. Catalano, V. Bartolomei, J. Labille, Release and fate of nanoparticulate TiO2 UV filters from sunscreen: Effects of particle coating and formulation type, Environ. Pollut. 271 (2021) 116263. doi:10.1016/J.ENVPOL.2020.116263.

[23] A. Rampaul, I.P. Parkin, L.P. Cramer, Damaging and protective properties of inorganic components of sunscreens applied to cultured human skin cells, J. Photochem. Photobiol. A Chem. 191 (2007) 138–148. doi:10.1016/J.JPHOTOCHEM.2007.04.014.

[24] N. Martin, B. Wassmur, D. Slomberg, J. Labille, T. Lammel, Influence of TiO2 nanocomposite UV filter surface chemistry and their interactions with organic UV filters on uptake and toxicity toward cultured fish gill cells, Ecotoxicol. Environ. Saf. 243 (2022) 113984. doi:10.1016/J.ECOENV.2022.113984.

[25] J. Hu, L. Yang, P. Yang, S. Jiang, X. Liu, Y. Li, Polydopamine free radical scavengers, Biomater. Sci. 8 (2020) 4940–4950. doi:10.1039/d0bm01070g.

[26] A. Bino, A. Baldisserotto, E. Scalambra, V. Dissette, D.E. Vedaldi, A. Salvador, E. Durini, S. Manfredini, S. Vertuani, Design, synthesis and biological evaluation of novel

hydroxy-phenyl-1H-benzimidazoles as radical scavengers and UV-protective agents, J. Enzyme Inhib. Med. Chem. 32 (2017) 527–537. doi:10.1080/14756366.2016.1265523.

[27] S.Q. Wang, Y. Balagula, U. Osterwalder, Photoprotection: a Review of the Current and Future Technologies, Dermatol. Ther. 23 (2010) 31–47. doi:https://doi.org/10.1111/j.1529-8019.2009.01289.x.

[28] S.R. Ghazali, N.H. Rosli, L.S. Hassan, M.Z. Helmi Rozaini, H. Hamzah, Biocompatibility of Hydroxyapatite (HAp) derived from clamshell as active ingredients in sunscreenproduct, IOP Conf. Ser. Earth Environ. Sci. 646 (2021) 012059. doi:10.1088/1755-1315/646/1/012059.

[29] A. Pal, K. Hadagalli, P. Bhat, V. Goel, S. Mandal, Hydroxyapatite—a promising sunscreen filter, J. Aust. Ceram. Soc. 56 (2020) 345–351. doi:10.1007/s41779-019-00354-2.

[30] A. Adamiano, F. Carella, L. Degli Esposti, C. Piccirillo, M. Iafisco, Calcium Phosphates from Fishery Byproducts as a Booster of the Sun Protection Factor in Sunscreens, ACS Biomater. Sci. Eng. 8 (2022) 4987–4995. doi:10.1021/acsbiomaterials.2c00680.

[31] F. Taraballi, S. Minardi, A. Kumar, F. Baino, S.S. Han, S. Kargozar, Additive Manufacturing Methods for Producing Hydroxyapatite and Hydroxyapatite-Based Composite Scaffolds: A Review, Front. Mater. 6 (2019) 313. doi:10.3389/fmats.2019.00313.

[32] E. Campodoni, M. Montanari, C. Artusi, G. Bassi, F. Furlani, M. Montesi, S. Panseri, M. Sandri, A. Tampieri, Calcium-Based Biomineralization: A Smart Approach for the Design of Novel Multifunctional Hybrid Materials, J. Compos. Sci. 5 (2021) 278. doi:10.3390/jcs5100278.

[33] A. Tampieri, T. D'Alessandro, M. Sandri, S. Sprio, E. Landi, L. Bertinetti, S. Panseri, G. Pepponi, J. Goettlicher, M. Bañobre-López, J. Rivas, Intrinsic magnetism and hyperthermia in bioactive Fe-doped hydroxyapatite, Acta Biomater. 8 (2012) 843–851. doi:10.1016/j.actbio.2011.09.032.

[34] E. Campodoni, Design and development of bio-hybrid multifunctional materials for

regenerative medicine, University of Parma, 2018. https://hdl.handle.net/1889/3763.

[35] J. Liu, S. Yang, X. Li, Q. Yan, M.J.T. Reaney, Z. Jiang, Alginate Oligosaccharides: Production, Biological Activities, and Potential Applications, Compr. Rev. Food Sci.

Food Saf. 18 (2019) 1859–1881. doi:10.1111/1541-4337.12494.

[36] D. Liu, M. Nikoo, G. Boran, P. Zhou, J.M. Regenstein, Collagen and Gelatin, Annu. Rev.

Food Sci. Technol. 6 (2015) 527–57. doi:10.1146/annurev-food-031414-111800.

[37] T. Yotsuyanagi, I. Yoshioka, N. Segi, K. Ikeda, Acid-Induced and Calcium-Induced

Gelation of Alginic Acid: Bead Formation and pH-Dependent Swelling, Chem. Pharm.

Bull. 39 (1991) 1072–1074. doi:10.1248/cpb.39.1072.

[38] A. Adamiano, N. Sangiorgi, S. Sprio, A. Ruffini, M. Sandri, A. Sanson, P. Gras, D.

Grossin, C. Francès, K. Chatzipanagis, M. Bilton, B. Marzec, A. Varesano, F. Meldrum,

R. Kröger, A. Tampieri, Biomineralization of a titanium-modified hydroxyapatite

semiconductor on conductive wool fibers, J. Mater. Chem. B. 5 (2017) 7608–7621.

doi:10.1039/c7tb00211d.

[39] C. Menale, E. Campodoni, E. Palagano, S. Mantero, M. Erreni, A. Inforzato, E. Fontana,

F. Schena, R. van't Hof, M. Sandri, A. Tampieri, A. Villa, C. Sobacchi, Mesenchymal

Stromal Cell-Seeded Biomimetic Scaffolds as a Factory of Soluble RANKL in Rankl-

Deficient Osteopetrosis, Stem Cells Transl. Med. 8 (2019) 22–34. doi:10.1002/sctm.18-

0085.

[40] E. Campodoni, S.M. Dozio, S. Panseri, M. Montesi, A. Tampieri, M. Sandri, Mimicking

Natural Microenvironments: Design of 3D-Aligned Hybrid Scaffold for Dentin

Regeneration, Front. Bioeng. Biotechnol. 8 (2020) 836. doi:10.3389/fbioe.2020.00836.

[41] X. Zhao, S. Ng, B.C. Heng, J. Guo, L. Ma, T.T.Y. Tan, K.W. Ng, S.C.J. Loo, Cytotoxicity

of hydroxyapatite nanoparticles is shape and cell dependent, Arch. Toxicol. 87 (2013)

1037–1052. doi:10.1007/s00204-012-0827-1. [42] European Commission, Scientific Committee on Consumer Safety (SCCS), Sci.

Committees. (2021) 1–81.

https://ec.europa.eu/health/scientific_committees/consumer_safety_en.

[43] I.M. Joni, L. Nulhakim, C. Panatarani, Characteristics of TiO2 particles prepared by simple solution method using TiCl3 precursor, J. Phys. Conf. Ser. 1080 (2018) 012042. doi:10.1088/1742-6596/1080/1/012042.

[44] P.O. Kuzema, O.N. Stavinskaya, I. V. Laguta, O.A. Kazakova, Thermogravimetric study of water affinity of gelatin materials, J. Therm. Anal. Calorim. 122 (2015) 1231–1237. doi:10.1007/s10973-015-4823-6.

[45] J.P. Soares, J.E. Santos, G.O. Chierice, E.T.G. Cavalheiro, Thermal behavior of alginic acid and its sodium salt, Eclet. Quim. 29 (2004) 53–56. doi:10.1590/s0100-46702004000200009.

[46] E. Landi, A. Tampieri, M. Mattioli-Belmonte, G. Celotti, M. Sandri, A. Gigante, P. Fava, G. Biagini, Biomimetic Mg- and Mg,CO3-substituted hydroxyapatites: synthesis characterization and in vitro behaviour, J. Eur. Ceram. Soc. 26 (2006) 2593–2601. doi:10.1016/J.JEURCERAMSOC.2005.06.040.

[47] C. Piccirillo, C. Rocha, D.M. Tobaldi, R.C. Pullar, J.A. Labrincha, M.O. Ferreira, P.M.L. Castro, M.M.E. Pintado, A hydroxyapatite-Fe2O3 based material of natural origin as an active sunscreen filter, J. Mater. Chem. B. 2 (2014) 5999–6009. doi:10.1039/c4tb00984c.

[48] S. Smaoui, H. Ben Hlima, I. Ben Chobba, A. Kadri, Development and stability studies of sunscreen cream formulations containing three photo-protective filters, Arab. J. Chem. 10 (2017) S1216–S1222. doi:https://doi.org/10.1016/j.arabjc.2013.02.020.

[49] A. Marucco, E. Carella, I. Fenoglio, A comparative study on the efficacy of differentprobes to predict the photo-activity of nano-titanium dioxide toward biomolecules, RSC Adv. 5 (2015) 89559–89568. doi:10.1039/c5ra14303a.

[50] I. Fenoglio, J. Ponti, E. Alloa, M. Ghiazza, I. Corazzari, R. Capomaccio, D. Rembges, S. Oliaro-Bosso, F. Rossi, Singlet oxygen plays a key role in the toxicity and DNA damage caused by nanometric TiO2 in human keratinocytes, Nanoscale. 5 (2013) 6567–6576. doi:10.1039/c3nr01191g.

[51] D. C. Hurum, A. G. Agrios, K. A. Gray, T. Rajh, M. C. Thurnauer, Explaining the Enhanced Photocatalytic Activity of Degussa P25 Mixed-Phase TiO2 Using EPR, J. Phys.

Chem. B. 107 (2003) 4545–4549. doi:10.1021/jp0273934.

[52] Q. Feng, K. Wei, S. Lin, Z. Xu, Y. Sun, P. Shi, G. Li, L. Bian, Mechanically resilient, injectable, and bioadhesive supramolecular gelatin hydrogels crosslinked by weak hostguest interactions assist cell infiltration and in situ tissue regeneration, Biomaterials. 101 (2016) 217–228. doi:10.1016/J.BIOMATERIALS.2016.05.043.

[53] A.D. Augst, H.J. Kong, D.J. Mooney, Alginate hydrogels as biomaterials, Macromol. Biosci. 6 (2006) 623–633. doi:10.1002/mabi.200600069.

[54] M.I. Neves, L. Moroni, C.C. Barrias, Modulating Alginate Hydrogels for Improved Biological Performance as Cellular 3D Microenvironments, Front. Bioeng. Biotechnol. 8 (2020) 665. doi:10.3389/fbioe.2020.00665.

[55] M.B. Łabowska, K. Cierluk, A.M. Jankowska, J. Kulbacka, J. Detyna, I. Michalak, A Review on the Adaption of Alginate-Gelatin Hydrogels for 3D Cultures and Bioprinting, Materials (Basel). 14 (2021) 1–28. doi:10.3390/ma14040858.

[56] K. Anselme, Osteoblast adhesion on biomaterials, Biomaterials. 21 (2000) 667–681. doi:10.1016/S0142-9612(99)00242-2.